Valence band structures of GaAs/AlAs lateral superlattices

1999 J. Phys.: Condens. Matter 11 2809

(http://iopscience.iop.org/0953-8984/11/13/015)

J. Phys.: Condens. Matter **11** (1999) 2809–2820. Printed in the UK PII: S0953-8984(99)99447-X

Valence band structures of GaAs/AlAs lateral superlattices

Shu-Shen Li, Bang-Fen Zhu and Jian-Bai Xia

National Laboratory for Superlattices and Microstructures, Institute of Semiconductors, Chinese Academy of Sciences, PO Box 912, Beijing 100083, People's Republic of China

Received 17 November 1998

Abstract. In the framework of effective-mass envelope function theory, the valence energy subbands and optical transitions in lateral superlattices (LSLs) have been calculated by the plane-wave expansion method. The effects of finite offset and valence band mixing are taken into account. The modulations of several types of lateral potential are also evaluated; they indicate that the out-of-phase modulation on either side of the wells is the strongest while the in-phase modulation is the weakest. The lateral modulation periods have a weak effect on the lowest hole energy levels. When one is making LSLs, the fabrication can be tailored to make the lateral modulation period fairly large, which is favourable for technological applications. Our calculations also show that the effect of the difference between the effective masses of holes in different materials on the valence subband structures is significant. Our theoretical results are in agreement with the available experimental data and have great significance as regards investigating and making low-dimensional semiconductor devices.

1. Introduction

Advanced crystal growth techniques such as molecular beam epitaxy (MBE) and metal–organic vapour-phase epitaxy have made it possible to fabricate semiconductor nanostructures which are precise on the atomic scale and in which the carrier motion is confined in one, two, or three spatial directions. The study of these low-dimensional quantum confined systems has attracted a great deal of attention in the past few years.

Lateral superlattices (LSLs) are made by imposing a periodic modulation on or in the lateral planes of quantum wells and superlattices. There are two classes of methods of fabricating LSLs. One is the conventional processing technologies which lead to a direct-patterning modulation structure on the surface of quantum wells as a result of physical or chemical processing. The smallest modulation period, on the 100 nm scale, has been achieved in the last decade by such processing technologies. The second class of methods of making LSLs evolves epitaxial growth of periodic structures in the lateral direction. The tilted superlattices and the fractional-layer superlattices, with characteristic lengths of 10 nm or less, belong to this class. Quantum wires may be regarded as the localization limit of LSLs.

Since the LSLs are ideal systems for use in investigating the effect of dimensionality crossover on the electric and optical properties of low-dimensional systems, and are useful in exploring the fabrication technology of quantum wires and dots, a great deal of experimental and theoretical research has been carried out on them in the past ten years [1–13]. However, until now, owing to the complicated potential pattern on the lateral planes, only a few calculations on the electronic subband structures have been carried out [14–18]. Sun [14] has recently calculated the minigaps between the first two electronic subbands in GaAs/AlAs

0953-8984/99/132809+12$19.50

LSLs by using a variational calculation based on the simple two-wave approximation—that is, the trial wave function is composed of products of the ground state of the quantum well and two plane waves in the lateral plane which differ by a reciprocal-lattice vector in the modulation direction. Such an approximation is qualitatively correct only when the modulation period is much larger than the well width. When the two length scales are comparable or the modulation period is much less than the well width, we obtain a quite different variation trend of the minigaps of LSLs for the structure described in reference [18].

Up to now, as far as we are aware, there have been no papers dealing with the valence subband structure in LSLs. In this paper, we intend to present a simple and efficient calculation model for the valence subband structure in LSLs. In the calculation, we will include the effect of finite offset and valence band mixing. Also, we will evaluate the effect of the difference between the effective masses of GaAs and AlAs on the valence subband energies in LSLs, which has been shown to be non-negligible for GaAs/AlAs superlattices.

2. The theoretical model

Let l and d be the average GaAs and AlAs widths of the LSLs, respectively; $L_z = l + d$ is the average period of the LSL along the growth direction of the LSLs, which is taken to be the z-direction. The interfaces between GaAs and AlAs are at

$$z = nL_z \pm (l/2) \pm f_{\pm}(x) \qquad (n = 0, \pm 1, \pm 2, \ldots)$$

where the $f_{\pm}(x)$ represent the periodic modulation structures on the lateral planes.

According to Burt and Foreman's effective-mass envelope function theory [19, 20], the effective-mass Hamiltonian of the holes can be written as follows:

$$H_h = H_0 + V_h(\boldsymbol{r}). \tag{1}$$

H_0 is the Foreman effective-mass Hamiltonian for the hole state (excluding spin–orbit splitting) [20] given by

$$H_0 = \frac{1}{2m_0}\begin{bmatrix} P_+ & R & -Q_- & 0 \\ R^+ & P_- & C^+ & -Q_+^+ \\ -Q_-^+ & C & P_- & -R \\ 0 & -Q_+ & -R^+ & P_+ \end{bmatrix} \tag{2}$$

where

$$\begin{aligned} P_{\pm} &= p_x(\gamma_1 \pm \gamma_2)p_x + p_y(\gamma_1 \pm \gamma_2)p_y + p_z(\gamma_1 \mp 2\gamma_2)p_z \\ Q_{\pm} &= 2\sqrt{3}\left[(p_x \pm \mathrm{i}p_y)(\sigma - \delta)p_z + p_z\pi(p_x \pm \mathrm{i}p_y)\right] \\ R &= \sqrt{3}\left[(p_x + \mathrm{i}p_y)\mu(p_x + \mathrm{i}p_y) - (p_x - \mathrm{i}p_y)\gamma(p_x - \mathrm{i}p_y)\right] \\ C &= 2p_z(\sigma - \delta - \pi)(p_x - \mathrm{i}p_y) - 2(p_x - \mathrm{i}p_y)(\sigma - \delta - \pi)p_z \end{aligned} \tag{3}$$

and

$$\begin{aligned} \sigma - \delta &= (-1 - \gamma_1 + 2\gamma_2 + 6\gamma_3)/6 \\ \pi &= (1 + \gamma_1 - 2\gamma_2)/6 \\ \gamma &= (\gamma_2 + \gamma_3)/2 \\ \mu &= -(\gamma_2 - \gamma_3)/2. \end{aligned} \tag{4}$$

γ_1, γ_2, and γ_3 are the Luttinger effective-mass parameters which are functions of x, y, z:

$$\gamma_1, \gamma_2, \gamma_3 = \begin{cases} \gamma_{11}, \gamma_{12}, \gamma_{13} & \text{for } -l/2 - f_-(x) < z - nL_z < l/2 + f_+(x) \\ \gamma_{21}, \gamma_{22}, \gamma_{23} & \text{elsewhere.} \end{cases} \tag{5}$$

γ_{11}, γ_{12}, γ_{13} and γ_{21}, γ_{22}, γ_{23} are the Luttinger effective-mass parameters of GaAs and AlAs, respectively. m_0 is the free-electron mass. V_h is the hole potential:

$$V_h(\boldsymbol{r}) = \begin{cases} 0 & \text{for } -l/2 - f_-(x) < z - nL_z < l/2 + f_+(x) \\ \Delta V_h & \text{elsewhere.} \end{cases} \tag{6}$$

The hole envelope function equation is

$$H_h \Psi = E\Psi. \tag{7}$$

To make further calculations, we must specify the periodical interface structure. As a model, we assume that

$$f_\pm(x) = \Delta l^\pm \cos\left(\frac{2\pi x}{L_x}\right) \tag{8}$$

where $\Delta l^\pm$ and L_x are the amplitude and period of the modulation structure. Our method can easily be extended to calculate the hole state in other LSLs with various potential shapes. When $\Delta l^- = 0$, equation (8) reduces to equation (11) of reference [14]. Clearly, the present model is more general than the model of reference [14]. Figures 1(a), 1(b), 1(c), and 1(d) show the four kinds of shape of the two adjacent faces in LSLs, respectively. We can define figure 1(a) and 1(b) as showing out-of-phase ($\Delta l^+ = \Delta l^-$) and in-phase ($\Delta l^+ = -\Delta l^-$) modulations, respectively. Figure 1(c) corresponds to the modulation structure of reference [14]. Figure 1(d) shows the case for ordinary superlattices without modulation.

Using the plane-wave expansion method, we assume that the hole wave functions have the following forms:

$$\Psi_h(\boldsymbol{r}_h) = \frac{1}{L_x L_z} \mathrm{e}^{\mathrm{i}k_y y} \sum_{nm} \begin{bmatrix} a_{nm} \\ b_{nm} \\ c_{nm} \\ d_{nm} \end{bmatrix} \mathrm{e}^{\mathrm{i}[(k_x + nK_x)x + (k_z + mK_z)z]} \tag{9}$$

with $K_x = 2\pi/L_x$, $K_z = 2\pi/L_z$, and $n, m = 0, \pm 1, \pm 2, \ldots$.

The matrix elements of Hamiltonian (1) for equation (9) can be written as

$$\begin{aligned}
(P_\pm)_{nm,m'n'} &= (\gamma_\pm^1 \delta_{nn'}\delta_{mm'} + \gamma_\pm^2 S_{nm,m'n'})(k_{nx}k'_{nx} + k_y k_y) \\
&\quad + (\gamma_\pm^3 \delta_{nn'}\delta_{mm'} + \gamma_\pm^4 S_{nm,m'n'})(k_{mz}k'_{mz}) \\
(Q_\pm)_{nm,m'n'} &= 2\sqrt{3}\left\{\left[(\sigma_1 - \delta_1)\delta_{nn'}\delta_{mm'} - (\sigma_1 - \delta_1 - \sigma_2 + \delta_2)S_{nm,m'n'}\right](k'_{nx} \pm \mathrm{i}k_y)k_{mz}\right. \\
&\quad \left. + \left[\pi_1 \delta_{nn'}\delta_{mm'} - (\pi_1 - \pi_2)S_{nm,m'n'}\right](k_{nx} \pm \mathrm{i}k_y)k'_{mz}\right\} \\
R_{nm,m'n'} &= \sqrt{3}\left\{\left[\mu_1 \delta_{nn'}\delta_{mm'} - (\mu_1 - \mu_2)S_{nm,m'n'}\right](k_{nx} + \mathrm{i}k_y)(k'_{nx} + \mathrm{i}k_y)\right. \\
&\quad \left. - \left[\gamma^1 \delta_{nn'}\delta_{mm'} - (\gamma^1 - \gamma^2)S_{nm,m'n'}\right](k_{nx} - \mathrm{i}k_y)(k'_{nx} - \mathrm{i}k_y)\right\} \\
C_{nm,m'n'} &= -2(\sigma_1 - \delta_1 - \pi_1 - \sigma_2 + \delta_2 + \pi_2)S_{nm,m'n'}\left[(k_{nx} - \mathrm{i}k_y)k'_{mz} - (k'_{nx} - \mathrm{i}k_y)k_{mz}\right] \\
(V_h(\boldsymbol{r}))_{nm,m'n'} &= V_h S_{nm,m'n'}
\end{aligned} \tag{10}$$

with

$$\begin{aligned}
k_{nx} &= (k_x + nK_x) & k_{mz} &= (k_z + mK_z) \\
k'_{nx} &= (k_x + n'K_x) & k'_{mz} &= (k_z + m'K_z) \\
\gamma_\pm^1 &= \gamma_{11} \pm \gamma_{12} & \gamma_\pm^2 &= (\gamma_{21} \pm \gamma_{22}) - \gamma_\pm^1 \\
\gamma_\pm^3 &= \gamma_{11} \mp 2\gamma_{12} & \gamma_\pm^4 &= (\gamma_{21} \mp 2\gamma_{22}) - \gamma_\pm^3
\end{aligned}$$

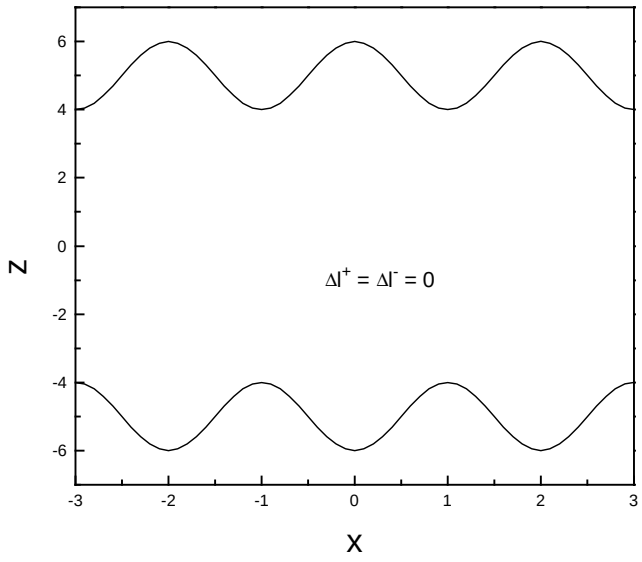

(a)

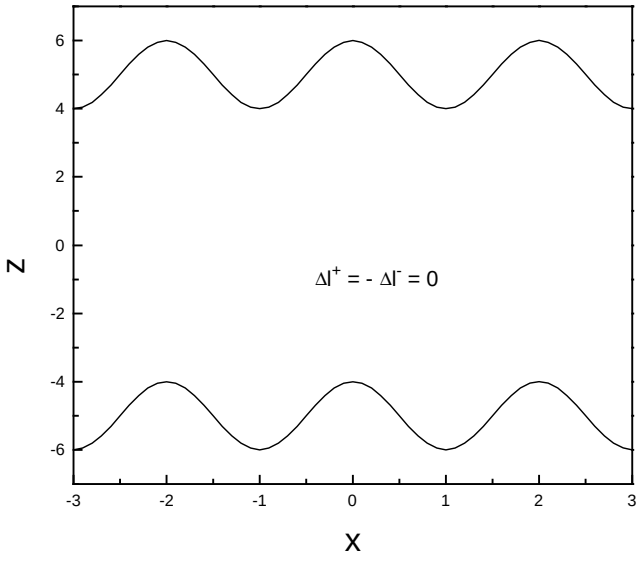

(b)

Figure 1. The four kinds of shape of the two adjacent faces in LSLs: $f_{\pm}(x) = \Delta l^{\pm}\cos(2\pi x/L_x)$. (a), (b), (c), and (d) correspond to out-of-phase modulations ($\Delta l^{+} = \Delta l^{-} \neq 0$), in-phase modulations ($\Delta l^{+} = -\Delta l^{-} \neq 0$), one-face modulations ($\Delta l^{+} \neq 0$ and $\Delta l^{-} = 0$), and an ordinary superlattice without modulations, respectively.

and

$$\sigma_i - \delta_i = (-1 - \gamma_{i1} + 2\gamma_{i2} + 6\gamma_{i3})/6 \qquad \pi_i = (1 + \gamma_{i1} - 2\gamma_{i2})/6$$
$$\gamma^i = (\gamma_{i2} + \gamma_{i3})/2 \qquad \mu_i = -(\gamma_{i2} - \gamma_{i3})/2$$
$$\sigma_i - \delta_i - \pi_i = (-1 - \gamma_{i1} + 2\gamma_{i2} + 3\gamma_{i3})/3$$

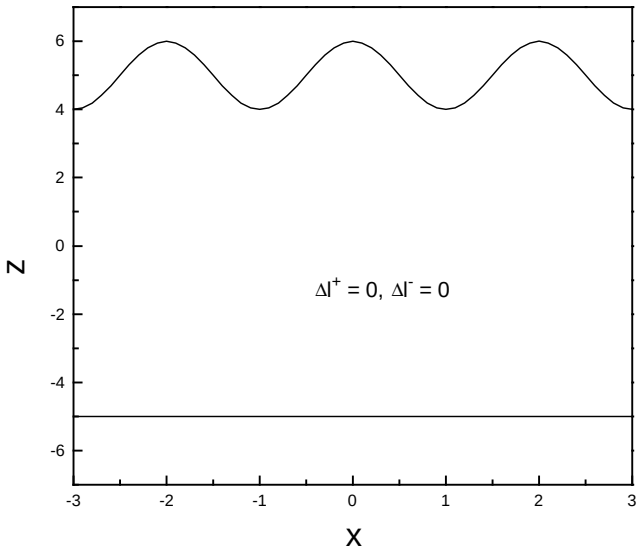

(c)

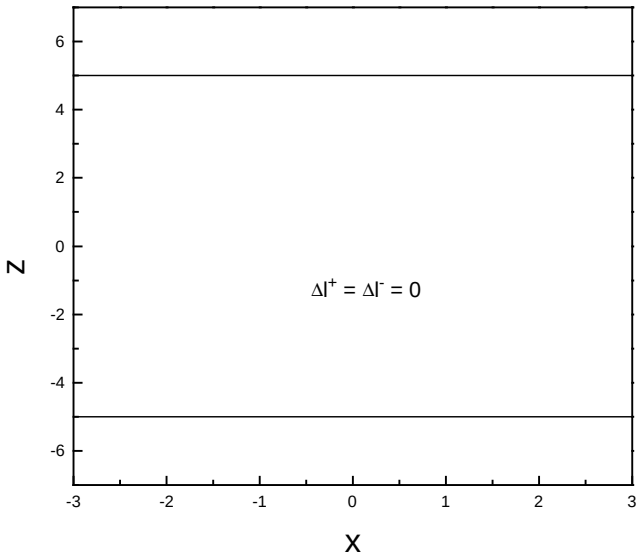

(d)

Figure 1. (Continued)

and $i = 1$ or 2. $\delta_{nn'}$ is a δ-function:

$$\delta_{nn'} = \begin{cases} 1 & \text{for } n = n' \\ 0 & \text{for } n \neq n'. \end{cases} \tag{11}$$

In equation (10), when $m \neq m'$,

$$S_{nm,m'n'} = \frac{\mathrm{i}}{2\pi(m - m')}(\mathrm{e}^{+}J^{+} - \mathrm{e}^{-}J^{-}) \tag{12}$$

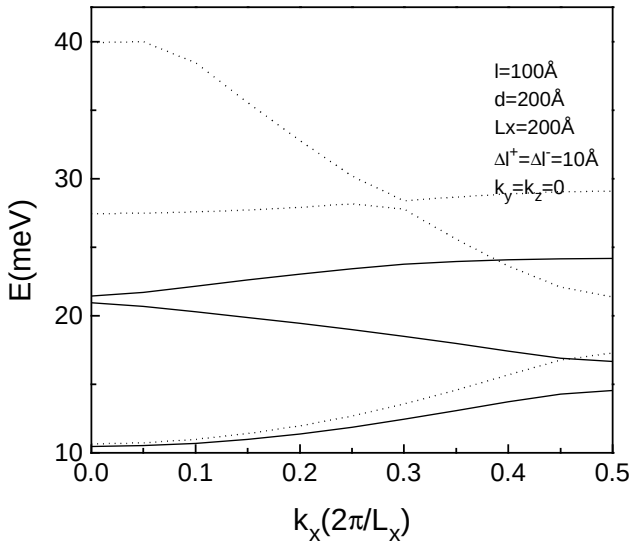

(a)

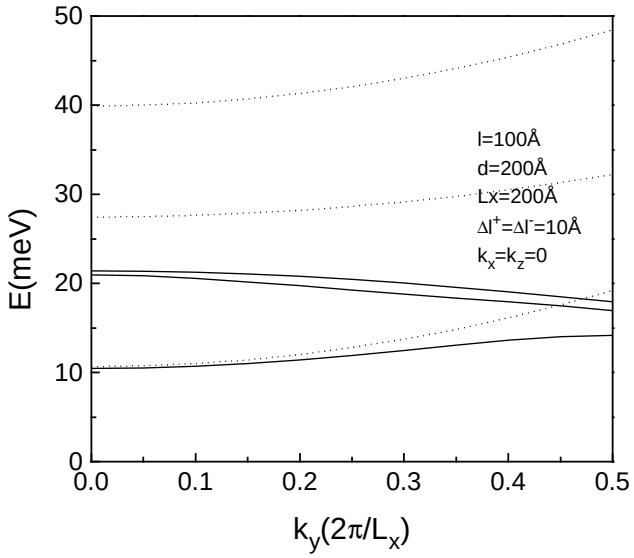

(b)

Figure 2. The lowest three subband energy dispersions of holes as functions of the wavenumber in the x-direction k_x (a), in the y-direction k_y (b), and in the z-direction (c) with $l = 100$ Å, $d = 200$ Å, $L_x = 200$ Å, and $\Delta l^+ = \Delta l^- = 10$ Å. The solid and dashed curves show the results obtained including and excluding valence band mixing between heavy holes and light holes, respectively.

with

$$e^{\pm} = \exp\{\pm i\pi[(m - m')l/L_z + (n - n')/2]\}$$

and

$$J^{\pm} = J_{n-n'}[2\pi(m - m')\Delta l^{\pm}/L_z]$$

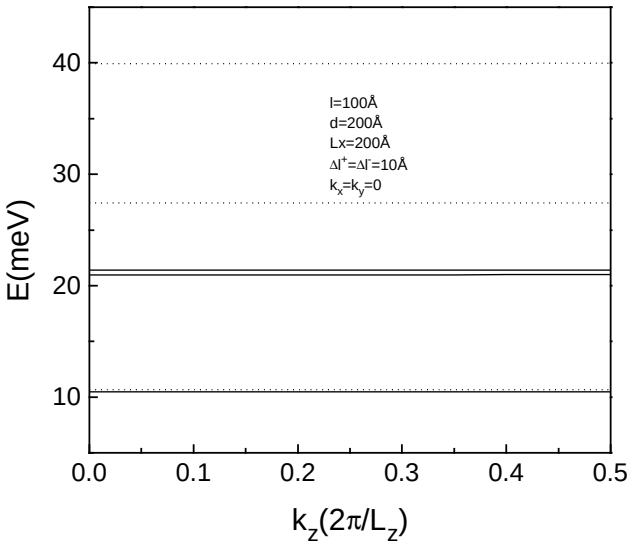

(c)

Figure 2. (Continued)

where $J_n(x)$ is the nth-order Bessel function of x. When $n = n'$ and $m = m'$,

$$S_{nm,m'n'} = \frac{d}{L_z}. \tag{13}$$

When $n - n' = \pm 1$ and $m = m'$,

$$S_{nm,m'n'} = -\frac{\Delta l^+ + \Delta l^-}{2L_z}. \tag{14}$$

And when $n - n' \neq 0$ or ± 1, and $m = m'$,

$$S_{nm,m'n'} = 0. \tag{15}$$

Thus, the valence subbands in LSLs can be worked out from equation (10).

3. Results and discussion

In our calculation, the bulk energy band-structure parameters of GaAs and AlAs are taken from reference [21] as shown in table 1. The valence band offset ΔV_h is taken to be 560.8 meV at the Γ point. The number of plane waves expanded in both x- and z-directions is 13 in our calculations—that is, $n, m = 0, \pm 1, \pm 2, \ldots, \pm 6$—and in terms of these, several of the lowest subbands can be accurately described.

Table 1. The energy band parameters of bulk GaAs and AlAs taken in our calculations

Material	E_g^Γ	γ_1	γ_2	γ_3
GaAs	1.5192	7.10	2.02	2.91
AlAs	3.14	3.94	0.76	1.53

In our model, it is easy to compare the confinement energies for four different modulation structures ($\Delta l^+ = \Delta l^- = 10$ Å, $\Delta l^+ = -\Delta l^- = 10$ Å, $\Delta l^+ = 10$ Å and $\Delta l^- = 0$, and

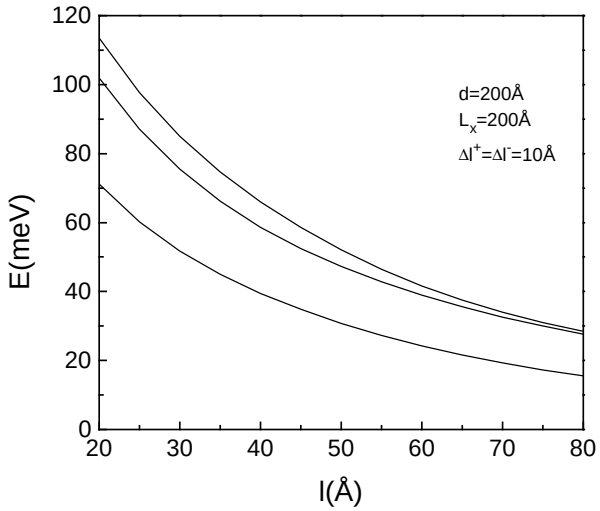

(a)

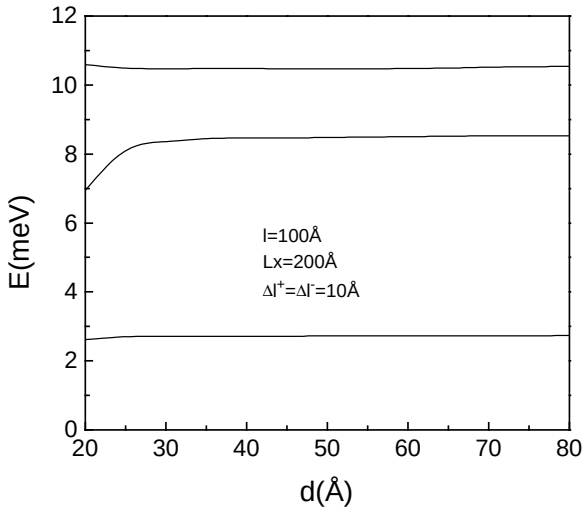

(b)

Figure 3. The lowest three hole energy levels at the Γ point as functions of the GaAs average thickness l (a), AlAs average thickness d (b), modulation period L_x (c), and modulation amplitude Δl (d).

$\Delta l^+ = \Delta l^- = 0$). Table 2 gives the lowest three hole energy levels at the Γ point with a fixed GaAs average thickness $l = 100$ Å, a fixed AlAs average thickness $d = 200$ Å, and a fixed modulation period $L_x = 200$ Å. The first hole level has larger confinement energy for two-face out-of-phase modulation ($\Delta l^+ = \Delta l^- = 10$ Å) and one-face modulation ($\Delta l^+ = 10$ Å and $\Delta l^- = 0$ Å), which is in contrast to the case for electrons [18]. This is due to the fact that holes have larger effective masses in AlAs than in GaAs.

In figure 2, we show the hole subband energy dispersion relations as functions of the hole wavenumber k and in the x-direction (figure 2(a)), in the y-direction (figure 2(b)), and in the z-direction (figure 2(c)), respectively, for samples with $l = 100$ Å, $d = 200$ Å, $L_x = 200$ Å,

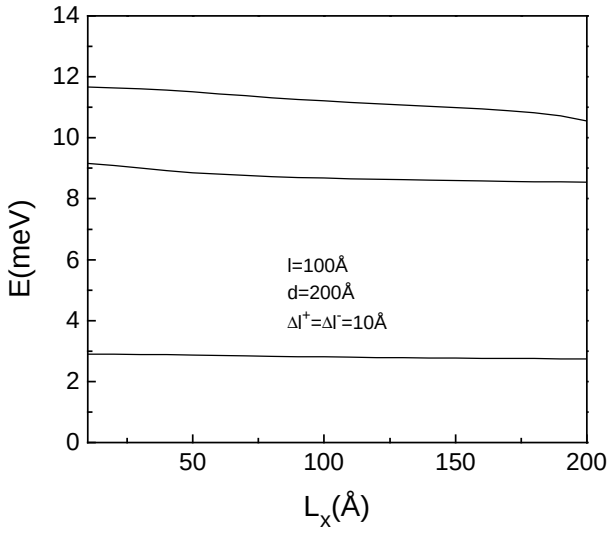

(c)

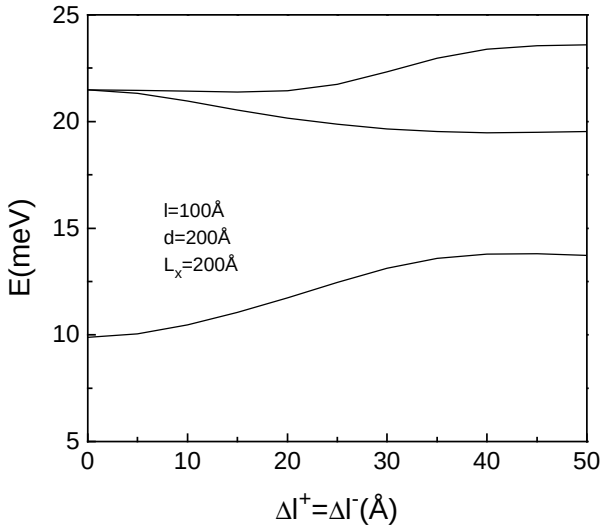

(d)

Figure 3. (Continued)

Table 2. The lowest three hole energy levels (meV) at the Γ point for GaAs/AlAs LSLs ($l = 100$ Å, $d = 200$ Å, $L_x = 200$ Å).

Δl (Å)	$\Delta l^+ = \Delta l^- = 10$	$\Delta l^+ = -\Delta l^- = 10$	$\Delta l^+ = 10$, $\Delta l^- = 0$	$\Delta l^+ = \Delta l^- = 0$
E_1	10.467	9.692	10.003	9.886
E_2	20.954	21.343	21.089	21.478
E_3	21.416	21.677	21.662	21.478

and $\Delta l^+ = \Delta l^- = 10$ Å. The solid and dashed curves are the results obtained including and excluding valence band mixing between heavy holes and light holes, respectively. For the

in-phase modulation and one-face modulation, there are similar trends; we have not shown the calculated results in figure 2. From our calculations, we found the following trends.

(a) As for the electron case [18], there are the minigaps between the hole subbands in LSLs. For the superlattices without modulation, the minigaps will disappear.
(b) Along the x- and y-directions, the energy dispersions are larger than those in the z-direction.
(c) The effects of valence band mixing are focused on high subbands.
(d) At the Γ point ($k_x = k_y = k_z = 0$), as in generally known, there is no valence band mixing for the superlattices without modulation. But for LSLs, there is also valence band mixing at the Γ point due to the lateral modulation.
(e) The anticrossings of hole levels are decreased in number by the effect of the valence band mixing (figure 2(a)).

Figures 3(a), 3(b), 3(c), and 3(d) show the lowest three hole energy levels at the Γ point as functions of the GaAs average thickness l, AlAs average thickness d, modulation period L_x, and modulation amplitude Δl, respectively. $l = 20$ Å in figure 3(a) and $d = 20$ Å in figure 3(b) are the cases of quantum well wires and quantum barrier wires, respectively. Figures 3(a) and 3(d) indicate that the well (GaAs) thickness l and modulation amplitude can strongly affect the lowest hole energy levels. The barrier (AlAs) thickness d and modulation period L_x have a weak effect on the lowest hole energy levels, as can be seen in figure 3(b) and 3(c), respectively. When one is making lateral structures, the fabrication can be tailored to make the lateral modulation period fairly large, which is favourable for technological applications. Due to the lateral modulation, there is a minigap between the second and the third hole energy levels at the Γ point. The minigap increases as the modulation amplitude increases, which can be seen in figure 1(d). From our calculation, we also found that the minigap between the first and the second hole energy levels appeared at $k_x = \pi/L_x$.

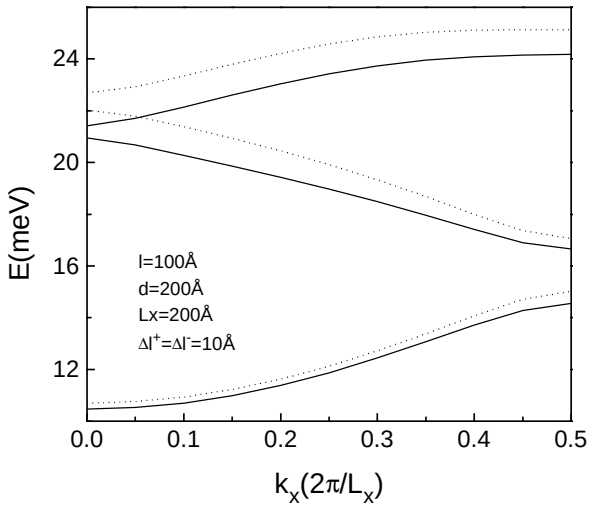

Figure 4. Hole subband energy dispersions at the Γ point as functions of the hole wavenumber in the x-direction k_x with $l = 100$ Å, $d = 200$ Å, $L_x = 200$ Å, and $\Delta l^+ = \Delta l^- = 10$ Å. The solid and dotted curves represent the results obtained taking account and without taking account of the difference between the effective masses in the well and barrier, respectively.

To examine the effect of the difference between the effective masses of the hole in the well and barrier materials on the energy subband dispersions, we have calculated the hole subband dispersions as functions of the hole wavenumber in the x-direction k_x with $l = 100$ Å, $d = 200$ Å, $L_x = 200$ Å, and $\Delta l^+ = \Delta l^- = 10$ Å. The results are shown in figure 4. The solid and dotted curves represent the results of taking different effective masses and taking the same effective masses (in GaAs), respectively. This figure shows that the different effective masses of holes in different materials significantly affect the subband dispersion, which can be as large as 0.2 meV for the first subband at $k_x = 0$ with the above structure parameters. The difference is even larger than 0.2 meV at other points of the reduced Brillouin minizone in the LSLs.

Notzel *et al* reported on the direct synthesis of superlattices with lateral corrugation of the interfaces on (311) GaAs substrates by MBE [22]. The structure was shown in figure 1 of reference [22]. The lateral corrugation can be simplified to a cosine function with $L_x = 32$ Å and $\Delta l^+ = \Delta l^- = 5.1$ Å. The first peak of the experimental photoluminescence was located at 1.605 eV. Our theoretical result is 1.619 eV. The theoretical value is higher than the experimental result by about 14 meV. The reason for this is probably that we have not taken into account the binding energy of the exciton.

4. Summary

Within the effective-mass envelope function theory and the plane-wave expansion formalism, the hole subband structure for GaAs/AlAs LSLs has been calculated. Among the three types of modulation studied in this paper, the out-of-phase modulation increases the quantum confinement most while the in-phase modulation has the weakest effect. The lateral modulation period has a weak effect on the lowest hole energy levels. Our calculation also indicates the importance of using realistic effective masses for GaAs and AlAs when calculating the subband dispersion. The conclusion of this paper has some significance as regards investigating and making low-dimensional semiconductor devices.

Acknowledgment

This work was supported by the National Natural Science Foundation of China under Grant No 69736010.

References

[1] Ploog K (ed) 1995 *III–V Quantum System Research (IEE Materials and Devices Series vol 11)* (New York: IEE) and references therein
[2] Göbel E O and Ploog K 1990 *Prog. Quantum Electron.* **14** 289 and references therein
[3] Brinkop F, Hansen W, Kotthaus J P and Ploog K 1988 *Phys. Rev.* B **37** 6547
[4] Demel T, Heitmann D, Grambow P and Ploog K 1988 *Phys. Rev.* B **38** 12 732
[5] Fukai T and Saito H 1988 *J. Vac. Sci. Technol.* B **6** 1373
[6] Tanaka M and Sakaki H 1988 *Japan. J. Appl. Phys.* **27** L2025
[7] Gerhardts R R, Weiss D and von Klitzing K 1989 *Phys. Rev. Lett.* **62** 1173
[8] Tsuchiya M, Gaines J M, Yan R H, Simes R J, Holtz P O, Coldren L A and Petroff P M 1989 *Phys. Rev. Lett.* **62** 466
[9] Gaines J M, Petroff P M, Kroemer H, Simes R J, Geels R S and English J H 1988 *J. Vac. Sci. Technol.* B **6** 1378
[10] Winkler R W, Kotthaus J P and Ploog K 1989 *Phys. Rev. Lett.* **62** 1177
[11] Kohl M, Heitmann D, Grambow P and Ploog K 1990 *Phys. Rev. Lett.* **42** 2941
[12] Stormer H L, Pfeiffer L N, Baldwin K W, West K W and Spector J 1991 *Appl. Phys. Lett.* **58** 726
[13] Shchukin V A and Efetov K B 1991 *Phys. Rev.* B **43** 14 164

[14] Sun H 1992 *Phys. Rev.* B **46** 12 371
[15] Jouanin C and Bertho 1994 *Phys. Rev.* B **50** 1645
[16] Li Shu-Shen and Xia Jian-Bai 1994 *Phys. Rev.* B **50** 8602
[17] Xia Jian-Bai and Li Shu-Shen 1995 *Phys. Rev.* B **51** 17 203
[18] Li Shu-Shen and Zhu Bang-Fen 1998 *J. Phys.: Condens. Matter* **10** 6311
[19] Burt M G 1992 *J. Phys.: Condens. Matter* **4** 6651
[20] Foreman B A 1995 *Phys. Rev.* B **52** 12 241
[21] Pavesi L and Guzzi M 1994 *J. Appl. Phys.* **75** 4779
[22] Notzel R, Ledentsov N N and Ploog K 1993 *Phys. Rev.* B **47** 1299